ACS APPLIED POLYMER MATERIALS

pubs.acs.org/acsapm Article

High-Throughput Manufacturing of Antibacterial Nanofibers by Melt Coextrusion and Post-Processing Surface-Initiated Atom Transfer Radical Polymerization

Justin D. Hochberg, David M. Wirth, Giovanni Spiaggia, Pooja Shah, Barbara Rothen-Rutishauser, Alke Petri-Fink, and Jonathan K. Pokorski*

Cite This: ACS Appl. Polym. Mater. 2022, 4, 260−269 Read Online

ACCESS | Metrics & More | Article Recommendations | Supporting Information

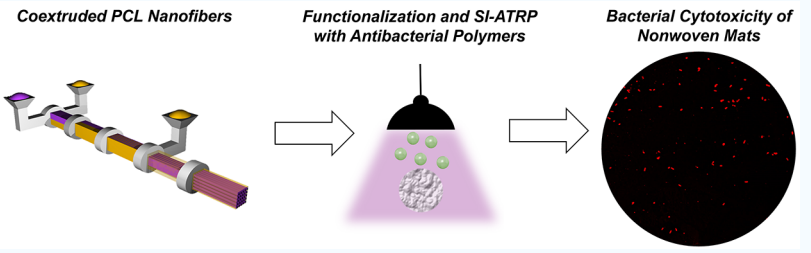

ABSTRACT: Polymeric nanofiber scaffolds are widely used for drug delivery, tissue engineering, and as advanced bandages. A high-throughput melt-processing method to fabricate polyester nanofibers was recently developed, as well as subsequent photochemical modification to generate functional fibers for use in tissue engineering and filtration. This work builds on these processes and details methods to develop antibacterial nanofiber mats. Melt coextrusion was used to fabricate poly(ε-caprolactone) (PCL) nanofibers. The isolated fibers could then be modified using *grafting-from* or *grafting-to* strategies to install antimicrobial polymers on their surfaces. The antimicrobial mats derived from the *grating-from* strategy demonstrated superior antimicrobial activity against Gram-positive and Gram-negative bacteria, while maintaining biocompatibility. The work developed herein provides a scalable method to fabricate advanced, functional, nonwoven mats that show potential for use as advanced bandages.

KEYWORDS: *nanofibers, melt coextrusion, SI-ATRP, antibacterial, biocompatibility*

1. INTRODUCTION

Polymeric nanofibers have recently gained significant attention because of their use as scaffolds in biomedicine, particularly in the areas of tissue engineering, drug delivery, and wound-healing.[1−4] Nanofibers have been fabricated using a variety of methods, including electrospinning,[5] melt electrospinning,[6] melt blowing,[7] rotary jet spinning,[8,9] and melt coextrusion.[10] The diversity of methods employed implies that there are both advantages and drawbacks with each approach. The most commonly used fabrication technique, however, is electrospinning due to its simplistic design and its ability to control fiber dimension down to the nanoscale.[5] The quality of electrospun fibers significantly depends on the processing parameters of the system,[11,12] and the manufacturing method displays a relatively low throughput.[13] Less common fiber fabrication techniques, such as melt electrospinning, need high voltage while providing low throughput, melt blowing does not easily produce nanoscale fibers, and rotary jet spinning produces fibers with poor mechanical properties.[4,14]

Melt coextrusion has recently emerged as a nanofiber fabrication method that yields fibers with tunable mechanical properties and cross-sectional dimensions and is a continuous, solvent-free process that can produce mechanically robust nanofibers at a rate of 2 kg h^{-1} when using a laboratory-scale extruder.[10,14,15] Melt coextrusion, therefore, offers a 10-fold increase in production rates as opposed to electrospinning nanofibers, which can only reach maximum production rates of 200 g h^{-1}, without the need for organic solvents.[13] Nanofibers from melt coextrusion have been used in a variety of applications including as a scaffold for filtration media[16] and as a platform for neural growth and differentiation.[17] These nanofibers can be made from most extrudable thermoplastic polymers; however, there are important considerations when designing biomedical materials. The primary focus for a biomaterial is its inherent biocompatibility, while secondary considerations may include mechanical properties or degradation kinetics, among others.[4] Polyesters such as poly(glycolic

Received: September 22, 2021
Accepted: November 23, 2021
Published: December 21, 2021

https://doi.org/10.1021/acsapm.1c01264
ACS Appl. Polym. Mater. 2022, 4, 260−269

acid) (PGA), poly(lactic acid) (PLA), and poly(ε-caprolactone) (PCL) are noncytotoxic and can even enhance cellular proliferation and differentiation upon chemical modifications.[18−20] PCL specifically has a slow hydrolytic degradation rate of 2−3 years, is nontoxic, and is extremely flexible, being able to reach >700% elongation at breakage.[21,22]

A promising area for future nanofiber use is antibacterial materials. These materials are a tool currently undergoing intensive research, and fibrous scaffolds could contribute significantly to a reduction in bacterial infections. According to the U.S. Centers for Disease Control and Prevention (CDC), more than 2.8 million infections and 35,000 deaths occur each year in the United States because of antibiotic resistance.[23] An important step to prevent unnecessary disease and untimely death is to prevent infections, traditional and antibiotic-resistant alike, from occurring in the first place. Furthermore, skin and soft tissue infections (SSTI) are one of the most common types of bacterial infections, where approximately 10% of hospitalizations in the United States are due to an SSTI.[24,25] Bacterial skin infections are commonly caused by *Streptococcus pyogenes* (*S. pyogenes*) or *Staphylococcus aureus* (*S. aureus*), including antibiotic-resistant strains such as methicillin-resistant *Staphylococcus aureus* (*MRSA*).[26]

Antibacterial materials have the potential to mitigate the risk of infection by killing sufficient skin-borne bacteria prior to SSTIs, which would ultimately reduce systemic infection. Three main methods exist in fabricating effective antibacterial materials: (1) biocide-releasing materials, (2) materials that cause physical damage to bacteria on contact, and (3) materials decorated with cations.[27]

Biocide-releasing materials are an effective method of killing bacteria because of their release of agents such as silver, triclosan and cyclodextrin,[28] or chitosan,[29,30] which are effective at killing both Gram-positive and Gram-negative bacteria. Silver nanoparticles have been both encapsulated within (poly(vinyl alcohol))[31] and attached to the surface of nanofibers,[32] the latter of which was shown to kill *Bacillus anthracis* (*B. anthracis*), *S. aureus*, and *Escherichia coli* (*E. coli*). Silver nanoparticles kill bacteria via the leaching of silver ions from the nanoparticle surface, which interrupts ATP production and DNA replication. Silver however, delays wound-healing by similarly causing irritation and binding to DNA, inhibiting replication in mammalian cells as well.[27,33]

Contact killing is a method of delivering a lethal mechanical force to bacteria.[34] Single-walled carbon nanotubes (SWCNT) have been used to kill bacteria in this manner. One such example is embedding SWCNTs into polysulfone nanofibers. As the weight percent of the CNTs increase from 0.1 to 1.0%, the amount of *E. coli* killed increased from 18 to 76%. However, bacterial toxicity levels out after about 15 min and does not completely eradicate the bacteria.[35]

The final common method to fabricate bactericidal surfaces is to decorate them with cationic amphiphiles such as positively charged proteins/polypeptides and quaternary ammonium functionalities. Antimicrobial peptides (AMPs) are one class of these agents and have been used as an effective means of killing antibiotic-resistant bacteria. They are small biopolymers consisting of 20−50 amino acids that selectively bind and kill pathogenic bacteria without harming eukaryotic cells when administered within a therapeutic limit.[36−39] AMPs typically exhibit a net cationic charge at physiological pH. Electrostatic interactions attract AMPs to bacteria,[37,40] while hydrophobic units on the AMPs disrupt the integrity of the bacterial membrane, leading to cell death.[39] AMPs have been used in a wide variety of applications, including incorporation into graphene−silver nanocomposites to disrupt biofilms[41] and to prevent growth and biofilm formation of anaerobes typically associated with oral diseases.[42] While AMPs show excellent antimicrobial activity, they are naturally produced in low amounts and are expensive to synthesize. To combat these challenges, many groups have synthesized polymers with similar amphiphilic properties to the AMPs.[39,43−46] These polymers are extremely effective, often killing greater than 99% of bacteria, including *Pseudomonas aeruginosa*, *E. coli*, *Vibrio cholerae*, and *S. aureus*.[43] Many of these polymers are also nontoxic to mammalian cells.[39]

This article describes the fabrication of antibacterial nanofiber mats via co-extrusion and postprocessing chemical functionalization. Mats were initially fabricated using PCL, followed by two surface modification strategies to generate materials with antibacterial properties. The first strategy used surface-initiated atom-transfer radical polymerization (SI-ATRP) to decorate the nanofiber surface with two different AMP-like antimicrobial polymers[39,43] that are known to kill both Gram-negative and Gram-positive bacteria. SI-ATRP can have a variety of applications that include grafting hydrophobic polymer brushes on both organic and inorganic substrates via a water-accelerated "paint-on" method[47] and fabricating zwitterionic polymer brushes with a controlled density and thickness on a polyacrylonitrile ultrafiltration membrane surface.[48] While *grafting-to* allows for more control over polymer properties, *grafting-from* typically allows for a higher grafting efficiency,[49] thus allowing a higher degree of antimicrobial activity per unit area of the nanofiber mats. We demonstrated that this *grafting-from* functionalization technique enhanced antibacterial activity when compared to a *grafting-to* method using the same polymers with varying molecular weights. Lastly, we demonstrated high cytocompatibility of polymer-modified fiber mats.

2. MATERIALS AND METHODS

2.1. Materials. Poly(ethylene oxide) (PEO)—POLYOX N80−200 kDa and POLYOX N10−100 kDa—were purchased from Dow Chemical. CAPA 6800 PCL-80 kDa was purchased from The Perstorp Group. 4-Hydroxybenzophenone was purchased from Acros Organics. 1-Bromohexane and tris(2-dimethylaminoethyl)amine (Me_6TREN) were purchased from Alfa Aesar. 2-(Dimethylamino)-ethylmethacrylate (DEAEMA) and *N*-(3-dimethylaminopropyl)-methacrylamide (DMAPMA) were purchased from Tokyo Chemical Industry (TCI). *N*-(3-Aminopropyl)methacrylamide hydrochloride (APMA) was purchased from Chemscene. α-Bromoisobutyryl bromide and copper(I) bromide were purchased from Aldrich Chemistry. Triethylamine (TEA) was purchased from VWR Life Science. OP50−1 *E. coli* were purchased from the University of Minnesota Caenorhabditis Genetics Center. CA-MRSA USA 300 was obtained from the Zhang laboratory in the Nanoengineering Department at UCSD. Luria-Bertani (LB) broth was purchased from Fisher BioReagents. Todd-Hewitt (TH) broth was purchased from BD Biosciences. Yeast extract powder was purchased from MP Biomedicals. Viability/cytotoxicity assay kit for bacteria live and dead cells [containing DMAO and Ethidium Homodimer III (EthD-III)] was purchased from Biotium. In vitro mouse fibroblasts NIH/3T3, Dulbecco's Modified Eagle Medium (DMEM), penicillin/streptomycin solution, iron fortified calf bovine serum (CBS), and L-glutamine solution were acquired from ATCC. Cytotoxicity Detection Kit for lactate dehydrogenase (catalyst, diaphorase/NAD+ mixture, and dye solution INT and sodium lactate) was obtained from Sigma-Aldrich. Gibco trypsin−ethylenediamine tetraacetic acid (EDTA) (0.25%),

https://doi.org/10.1021/acsapm.1c01264
ACS Appl. Polym. Mater. 2022, 4, 260−269

phenol red, 4′,6-diamidino-2-phenylindole, and dihydrochloride (DAPI) were acquired from ThermoFisher Scientific. TGF-beta 1 DuoSet enzyme-linked immunosorbent assay (ELISA) kit and recombinant mouse interferon-γ (IFN-γ) were both purchased from R&D Systems, Inc.

2.2. Instrumentation and Equipment. PEO was blended in a Haake Rheodrive 5000 twin-screw extruder. Multilayer coextrusion was conducted on a custom-built, two-component system with a series of horizontal and vertical multipliers at Case Western Reserve University. A SereneLife SLPRWAS26 Compact Pressure Washer was used to remove excess PEO and entangle nanofibers to form mats. A CellScale Univert uniaxial testing apparatus was used for tensile tests. Nanofiber mats were shaped into a circular patch shape with Anytime Tools sharp 7/16″ hollow punch. Illumination for benzophenone photo-insertion was conducted with an Omnicure Model S1500 standard filter 320−500 nm UV light source. Scanning electron microscopy (SEM) images were collected with an FEI Apreo LoVac FESEM while energy-dispersive spectroscopy (EDS) data were collected with an Oxford Instruments X-Max 80 EDS detector. Water contact angle (WCA) measurements were taken with a ramé-hart Model 200 goniometer. X-ray photoelectron spectroscopy (XPS) data were collected with a Kratos Analytical AXIS Supra surface analysis instrument. Nuclear magnetic resonance (NMR) data were collected with either a 300 or 600 MHz Bruker Avance III spectrometer. Optical density (OD) measurements were taken using a BioTek Synergy HT microplate reader. Confocal microscopy images were taken with Leica SP8 and Zeiss LSM 710 meta confocal microscopes. The absorbances of lactate dehydrogenase (LDH) and TGF-beta1 DuoSet ELISA assays were measured with a Bio-Rad Plate reader. Cells were counted using an EVE automated cell counter.

2.3. Methods. *2.3.1. Melt Coextrusion of PCL/PEO Fiber Tapes.* As previously described, two different molecular weights (200 kDa/100 kDa) of PEO in a 30/70 w/w% ratio were compounded to provide a rheological match to PCL at the coextrusion temperature.[14] PEO was dried prior to use at 40 °C for 48 h. Compounding was performed in a twin-screw extruder set to 140 °C, and the extrudate was then pelletized.[17] PEO and PCL pellets were then dried for an additional 48 h at 40 °C. PCL fibers were then coextruded into a PEO matrix at 180 °C. The extrusion line consisted of 16 vertical and 4 horizontal multipliers and an encasement in a 33% PEO skin layer and exited through a 3″ tape die. The extruded tape was then collected on a chill roll at room temperature rotating at roughly 15 rpm.[16]

2.3.2. Removal of PEO To Form Nonwoven PCL Mats. PEO/PCL tapes were secured in a beaker of stirring water. Water was replaced every hour for 6 h. Fibers were then left overnight in a 70% MeOH/30% H_2O solution to remove PEO. Fibers were fixed to a fiberglass plate and covered with a wire mesh. Fibers were then washed with a pressure washer at its widest spray setting to remove the remaining PEO and entangle fibers. Fibers were punched into an 11 mm diameter circular shape with a hollow punching apparatus for subsequent chemical modifications.

2.3.3. Fiber Photochemistry. Fiber mats (11 mm diameter, approximately 8 mg) were dipped into a 10 mg/mL solution of the benzophenone-ATRP initiator in methanol (*grafting-from*) or a 5 mg/mL solution of polymer in methanol (*grafting*-to) and dried overnight in a vacuum desiccator. Fibers were then subjected to a broadband 320−500 nm UV light with an intensity of 548 $\frac{mW}{cm^2}$ for 45 min per side. Following UV exposure, mats were washed with methanol and dried again overnight in a vacuum desiccator. Successful fiber functionalization was confirmed via XPS and SEM−EDS. Both initiator-functionalized and *grafting-to* fibers were characterized via the WCA.

2.3.4. Grafting-from ATRP. Monomer (1.39 mmol), Me_6TREN (4.8 mg, 0.027 mmol), dimethylformamide (1 mL), and eight modified mats from Section 2.3.6 were added to a flame-dried three-neck round-bottom flask and purged with N_2. After 45 min, Cu(*I*)Br (2.0 mg, 0.014 mmol) is added under positive pressure, and the reaction is left to proceed overnight at room temperature. Fibers were then removed and placed in an Erlenmeyer flask with MeOH and stirred for 1 h, followed by vacuum-drying in a desiccator. Successful polymerization was confirmed via XPS and the WCA.

2.3.5. Synthesis of Photoreactive QA Polymer for Grafting-to. QA monomer (225 mg, 0.695 mmol), Me_6TREN (2.4 mg, 0.014 mmol), dimethylformamide (0.45 mL), and benzophenone initiator (QA-small: 4.8 mg, 0.014 mmol; QA-medium: 2.4 mg, 0.007 mmol, QA-large: 1.2 mg, 0.03 mmol) were added to a flame-dried three-neck round-bottom flask and purged with N_2. After 45 min, Cu(*I*)Br (1.0 mg, 0.007 mmol) was added under positive pressure. Polymerization was left overnight at room temperature. Polymers were dialyzed in deionized water for 2 days, followed by lyophilization.

2.3.6. Synthesis of Photolabile M30 Polymer for Grafting-to. APMA (50 mg, 0.280 mmol), DMAPMPA (28.0 mg, 0.164 mmol), Me_6TREN (1.5 mg, 0.009 mmol), dimethylformamide (0.45 mL), and benzophenone initiator (M30-small: 3.1 mg, 0.009 mmol; M30-medium: 1.5 mg, 0.004 mmol, M30-large: 0.8 mg, 0.002 mmol) are added to a flame-dried three-neck round-bottom flask and purged with N_2. After 45 min, Cu(*I*)Br (0.6 mg, 0.004 mmol) is added under positive pressure. Polymerization was left overnight at room temperature. Polymers were dialyzed in deionized water for 2 days, followed by lyophilization.

2.3.7. Bacterial Growth Measurements. *E. coli* and *MRSA* were cultured in LB broth and TH broth, respectively. *E. coli* with an OD at 600 nm (OD600) of 0.01 was incubated for 24 h at 37 °C with an 11 mm diameter polymer-modified mat cut in half in 500 μL of LB broth in a 48-well plate. *MRSA* were similarly prepared with an OD600 of 0.025 and incubated for 24 h at 37 °C with two 11 mm diameter polymer-modified mats in 750 μL of TH broth supplemented with yeast extract in a 48-well plate. OD readings were taken at 1, 3, 6, 12, and 24 h to show bacterial growth.

2.3.8. Bacterial Live/Dead Assay. Mats were incubated with bacteria, as previously described in Section 2.3.10. After 24 h, mats were removed from bacteria and treated with 70 μL of viability/cytotoxicity assay solution consisting of 9.1% DMAO, 18.2% EthD-III, and 72.7% 150 mM NaCl in sterile, deionized water for 15 min. Mats were then placed on glass microscope slides and imaged via confocal laser scanning microscopy scanning emissions at 530 nm (live cells) and 625 nm (dead cells).

2.3.9. Fibroblast Culture on Antimicrobial Mats. Mouse fibroblasts (NIH/3 T3) were cultivated in DMEM supplemented with 10 vol % CBS, 1 vol % penicillin/streptomycin, and 1 vol % of L-glutamine (cDMEM). NIH/3 T3 were grown in T75 flasks maintained at 37 °C, with a relative humidity of 95% and 5% of CO_2, until reaching 80% confluency. Cells were then washed with phosphate-buffered saline (PBS) (10 mL) and trypsinized with 1.5 mL of trypsin for 5 min. cDMEM (3 mL) was added to the cells, which were counted using an automatic cell counter. Punctured mats of 32 mm^2 in surface area were placed in 96-well plates and covered with approximately 20,000 cells (625 cells/mm^2) in 0.3 mL of cDMEM. Control experiments without mats were also performed by growing cells in 96-well plates.

2.3.10. LDH Assay. Cellular viability was assessed by measuring the release of LDH into the supernatant as a result of cell membrane rupture using an LDH cytotoxicity detection kit at 24 and 48 h of cell cultivation. At these time points, 100 μL supernatants were collected from NIH/3 T3 cultured on antimicrobial mats, as previously described in Section 2.3.12. Control cell cultures treated with 0.3 mL of 0.2 v/v % Triton X-100 in PBS served as a positive control for the LDH assay. Aliquots (100 μL) of each sample and 100 μL of the LDH assay kit were placed in a new 96-well plate. The absorbance at 630 nm of each sample was measured. The data of each measurement were normalized by the mean of the positive control's values.

2.3.11. Profibrotic Response. Transforming growth factor-β1 (TGF-β1) released into the supernatants by cells was quantified using the ELISA DuoSet Development diagnostic kit, following the manufacturer's protocol at 24 and 48 h of cultivation. Interferon gamma (1 μg/mL) in cDMEM was used as a positive control.

2.3.12. Cellular Proliferation. Following 24 and 48 h of cell growth, the cells were trypsinized with 100 μL of trypsin for 5 min and counted using an automatic cell counter. To confirm the

https://doi.org/10.1021/acsapm.1c01264
ACS Appl. Polym. Mater. 2022, 4, 260−269

effectiveness of the trypsinization procedure, mats were visualized by confocal microscopy to confirm 100% cell detachment. Samples were then washed three times with PBS and fixed with a 4 vol % solution of paraformaldehyde for 15 min. After three additional washes, mats were immersed in DAPI (1:100 dilution in PBS) for 5 min to detect still adherent fibroblasts.

2.4. Statistical Analysis. For the ELISA, LDH, and cell proliferation analyses, three independent experiments were performed (three biological replicates). Statistical analysis was performed using GraphPad Prism 6 (GraphPad Software Inc., La Jolla, CA, USA) software. A parametric one-way analysis of variance (ANOVA) was performed. Results were considered significant if $p < 0.05$.

3. RESULTS AND DISCUSSION

3.1. Melt Coextrusion and Fiber Mat Formation. PCL was chosen as the nanofiber material because of its biocompatibility, ductility, and ease of postextrusion chemical modification. Melt coextrusion proceeded, as previously described[17] and will be briefly described here. Coextrusion begins by stacking PEO and PCL melts in layers oriented vertically to one another. This is followed by a 90° rotation that forces the melt flows side-by-side (Figure 1.1). The flow

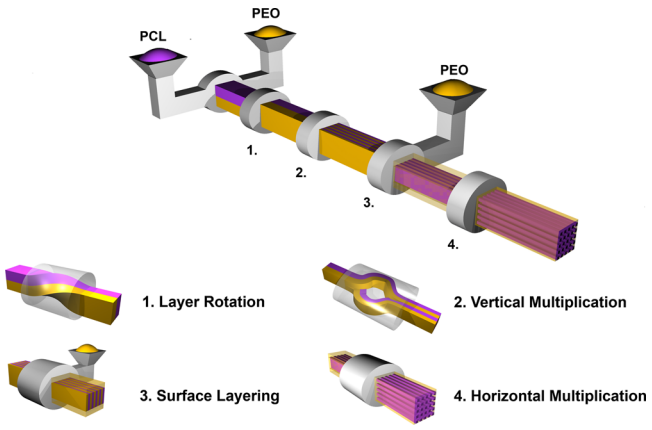

Figure 1. Schematic of melt coextrusion equipment and process featuring (1.1) layer rotation, (1.2) vertical multiplication, (1.3) surface layering, and (1.4) horizontal multiplication steps.

then feeds into a series of vertical multipliers; each multiplier doubles the number of layers; thus, "n" number of multipliers results in 2^{n+1} total vertical layers (Figure 1.2). Following vertical layer multiplication, a 33% skin layer of PEO is pumped on the top and bottom of the melt (Figure 1.3), which is finally followed by a series of horizontal multipliers (Figure 1.4). This horizontal multiplication creates nanoscopic separated domains of PCL embedded within the PEO matrix, yielding 2^m horizontal layers and 2^{n-m} vertical layers. This study used 16 vertical and 4 horizontal multipliers, producing 4096 × 16 PCL domains, results that were previously verified to be in the nanoscale regime.[50]

The resulting composite tapes were washed in a water bath for 6 h, with the bath being replaced every hour, followed by a 70% MeOH bath overnight to remove PEO. Fiber preparation was completed using a high-pressure water jet treatment, yielding a 98% removal of PEO (Figure S1). This step also served to entangle the fibers to create a nonwoven mat. These fiber mats were then stamped into circular mats with a diameter of 11 mm. SEM studies of fiber dimensions indicate a thickness of 0.78 ± 0.20 μm and a width of 0.38 ± 0.07 μm, averaged over 50 locations (Figure 2)A–D. Uniaxial tensile testing of fiber mats demonstrated mechanical properties that were similar to our previously reported values,[14] displaying an elastic modulus (E_T) of 50.6 ± 16.9 MPa and a yield strength (σ) of 8.1 ± 0.8 MPa (Figure 2E). Archimedes' principle of buoyancy was used to determine that the porosity of the nanofiber mats was 76.2 ± 3.9%, which is comparable to similar PCL nanofiber mats made via coextrusion.[16] The high porosity of our materials would be critical if applied for wound-healing because a highly porous system would allow for nutrient and gas exchange.[16]

3.2. Functionalization of Nanofibers via SI-ATRP. For functional polymers onto the nanofiber surface, we pursued two strategies, a *grafting-from* and a *grafting-to* approach (Figure 3A,B). A benzophenone-modified ATRP initiator was synthesized for *grafting-from* modification (Figures S2 and S3). The benzophenone moiety is known to undergo a photo-initiated insertion into the PCL backbone for covalent modification of the fiber surface (Figure 3A).[51] Upon photochemical modifications, an ATRP initiator remains exposed on the fiber surface. SI-ATRP can then be used as a means of *grafting-from* the fiber with antimicrobial polymers.[52] The distinct incorporation of bromine from the initiator allows for the confirmation of this attachment using a variety of methods including SEM–EDS (Figure S4) and XPS, and a change in the WCA is also seen from the unmodified nanofiber.

The modified fiber mats were used to initiate ATRP with a selection of cationic amphiphilic antibacterial (QA)[43] and (M30)[39] monomers, as well as a control monomer (PEGMEA) (Figures 3C and S5). QA and M30 are both cationic amphiphiles with AMP-like properties. QA is

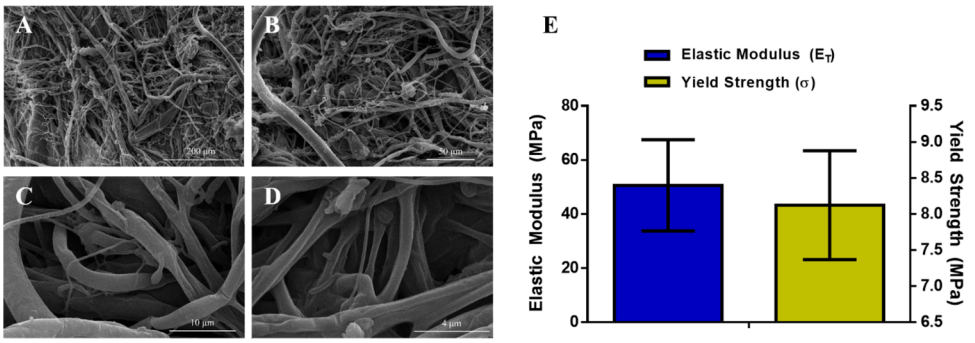

Figure 2. (A–D) Scanning electron micrograph of the PCL nanofiber mat at various magnifications. Scale bar indicates (A) 200 μm, (B) 50 μm, (C) 10 μm, and (D) 4 μm; (E) elastic modulus and yield strength of nanofiber mats.

https://doi.org/10.1021/acsapm.1c01264
ACS Appl. Polym. Mater. 2022, 4, 260–269

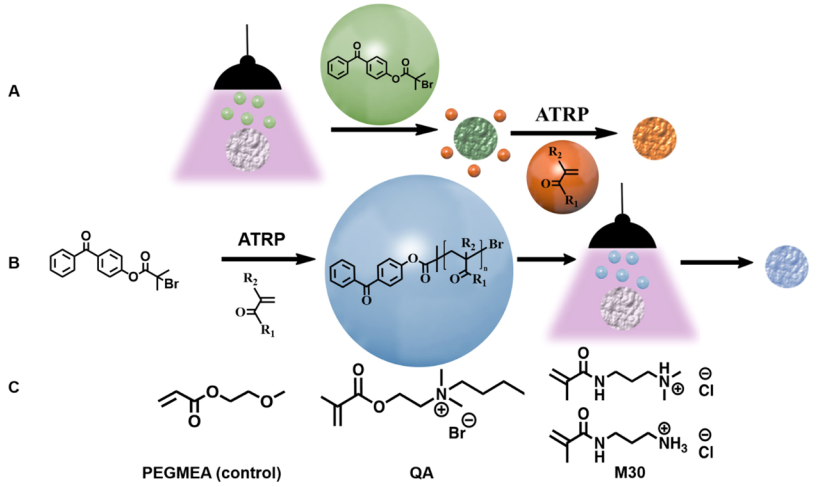

Figure 3. (A) Schematic diagram of *grafting-from* nanofiber mat functionalization. Mats are first exposed to the initiator under UV light. Mats then undergo ATRP to functionalize them with polymers. (B) Schematic diagram of *grafting-to* nanofiber mat functionalization. Polymers are first synthesized via ATRP. Mats are then exposed to reactive polymer under UV light. (C) Chemical structures of monomers used mat functionalization.

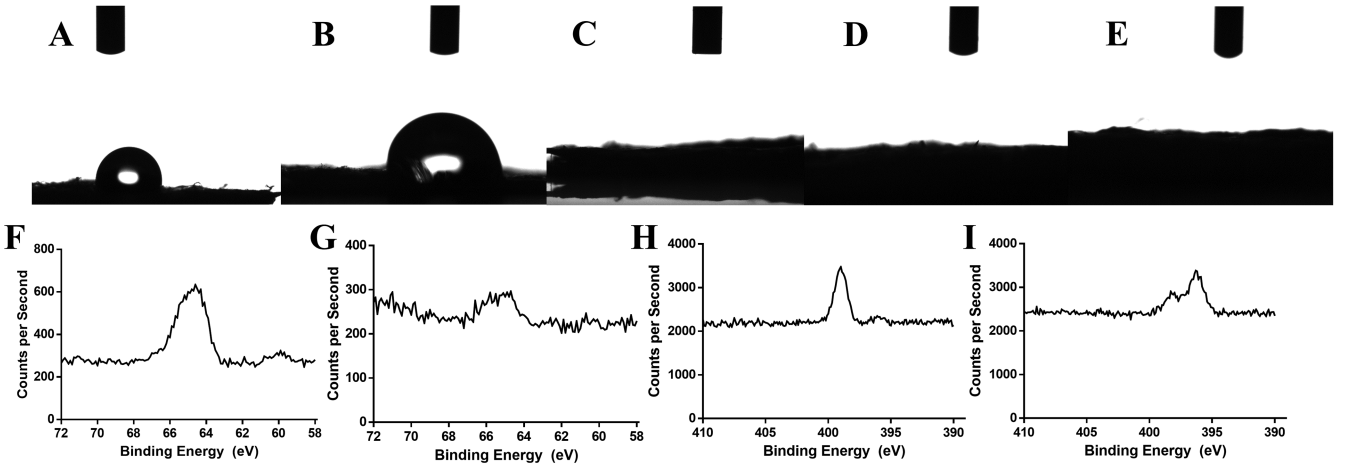

J

Fiber Sample	Percent Composition					WCA
	C	O	N	Br	Cl	
Unmodified PCL	61.1	38.9	0.0	0.0	0.0	83.7 ± 0.6°
Initiator	65.4	33.8	0.0	0.8	0.0	73.4 ± 1.6°
PEGMEA	49.1	50.8	0.0	0.1	0.0	0.0°
QA	59.3	35.0	2.1	3.6	0.0	0.0°
M30	55.1	39.8	1.9	1.9	1.3	0.0°

Figure 4. Surface characterization of functionalized nanofiber mats. WCA measurements of (A) PCL, (B) initiator-functionalized, (C) PEGMEA, (D) QA, and (E) M30 nanofiber mats. High-resolution XPS spectra of Br3d on (F) initiator-functionalized and (G) PEGMEA nanofiber mats. High-resolution XPS spectra of N1s on (H) QA- and (I) M30-functionalized nanofiber mats. (J) Table of elemental composition from XPS and WCAs of nanofiber mats.

methacrylate-based and contains a positively charged quaternary amine, while M30 is a methacrylamide-based copolymer containing units with both positively charged primary and tertiary amines. The rationale for the M30 copolymer is the increased bactericidal activity of a primary amine, while the more hydrophobic tertiary amine decreases eukaryotic cytotoxicity. Both polymers have been shown to have bactericidal effectiveness against Gram-positive and Gram-negative bacteria. We chose these polymers because of their antibacterial efficacy and chemical compatibility with our desired synthetic methods.

Following ATRP, the mats were characterized using WCA, a simple method to determine the surface energy between samples with differing chemistry. A slight decrease in WCA, 83.7 ± 0.56° to 73.4 ± 1.55°, was observed upon functionalization of the PCL mat with the ATRP initiator (Figure 4A,B). The decrease in the contact angle is due to an increased hydrophilicity of the fibers upon the covalent attachment of the ATRP initiator. Following polymerizations, all fibers showed complete and immediate wetting (0°) (Figure 4C–E), attributed to the hydrophilicity of the PEG groups in

https://doi.org/10.1021/acsapm.1c01264
ACS Appl. Polym. Mater. 2022, 4, 260−269

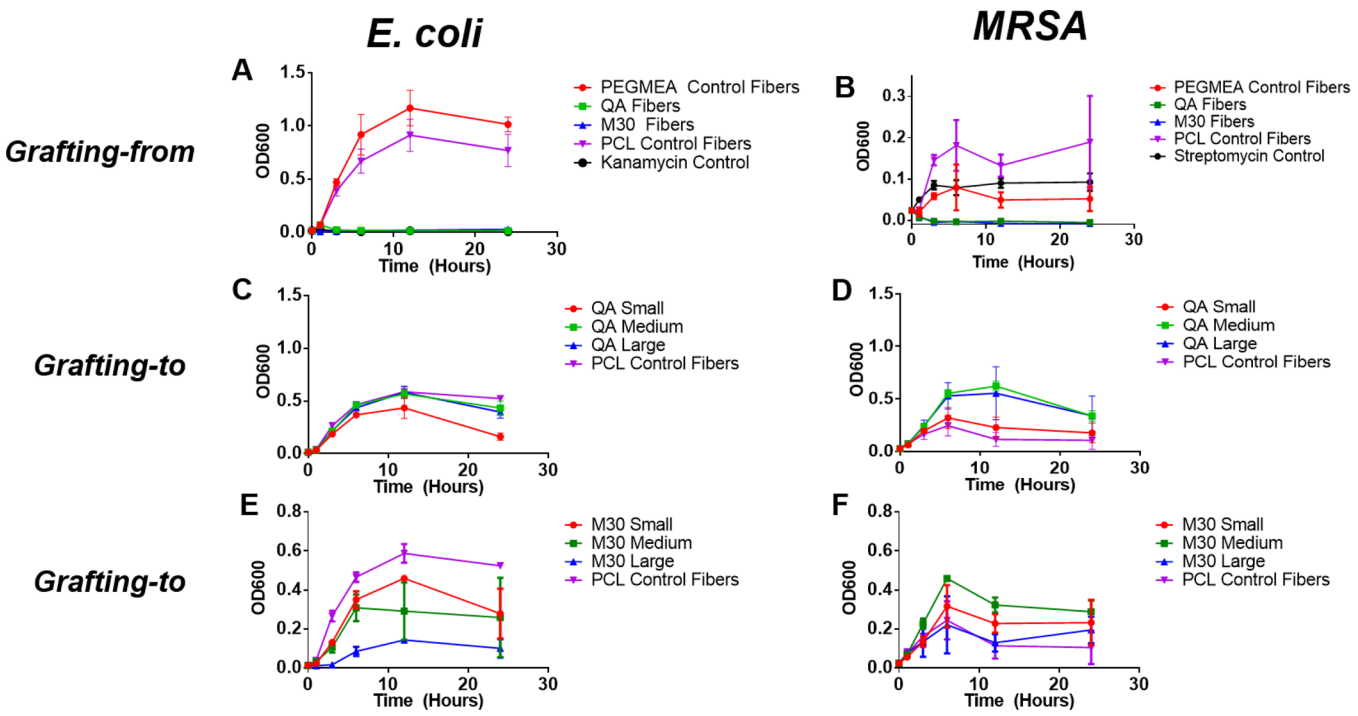

Figure 5. Optical density measurements at λ = 600 nm of incubations of (A,C,E) with *E. coli* and (B,D,F) with *MRSA*. (A,B) contain *grafting-from* mats while (C−F) contain *grafting-to* mats.

the PEGMEA-functionalized mats and the charged moieties in both the QA and M30 polymer-modified mats.

XPS was further used to characterize all fibrous samples to give information regarding the chemical makeup of the surface pre- and postfunctionalization. XPS further demonstrated the incorporation of bromine into the initiator-modified mats (Figure 4F), as evidenced by the presence of a bromine peak at 65 eV, characteristic of an electron being ejected from the 3d electron shell of a bromine atom. PEGMEA (Figure 4G) also shows a bromine peak that is correlated to the end group of the polymer, but with a lower intensity than that shown in Figure 4F because of the significantly increased proportion of carbon and oxygen atoms introduced upon functionalization with a PEG-containing monomer. QA and M30 polymers both contain nitrogen in their monomer units, making this a unique signal for functionalization. QA-functionalized mats demonstrate a single nitrogen peak at 399 eV, and M30 mats have two unique peaks between 395 and 399 eV (Figure 4H,I). QA-functionalized mats contain a single nitrogen peak because one distinct nitrogen appears in its chemical structure. M30-functionalized mats contain two separate nitrogen peaks because of its composition of two chemically unique nitrogen atoms. The M30 cationic nitrogen is at a higher binding energy than its amide nitrogen. QA-functionalized mats also feature a higher percentage of bromine as compared to the other mats because bromine is a counterion. Likewise, M30 mats have a lower bromine content because of their chlorine counterion. All surface characterization is summarized in Figure 4J.

Thermogravimetric analysis (TGA) further confirms the functionalization of the nanofiber mats, indicating a mass loss in the QA and M30 mats at ~200 °C. QA mats observe a 4.5% mass loss while M30 mats observe a 4.8% mass loss prior to the complete degradation of PCL when compared to the control PCL mats. Finally, SEM studies were conducted on the QA and M30 mats to verify the morphology, following chemical functionalization; there are no noticeable changes to the polymer-functionalized fibers (Figure S7).

3.3. Grafting-to Chemistry. As a comparison to the *grafting-from* method, antibacterial activity was compared with QA and M30 polymers conjugated to the PCL nanofiber mats via a *grafting-to* approach. *Grafting-to* chemistries are typically associated with a lower grafting efficiency than *grafting-from* chemistries. As such, we were interested in investigating how this would affect the bactericidal capabilities of our nanofiber mats. QA and M30 polymers were synthesized under standard solution-based ATRP conditions using our benzophenone-based initiator in solution. Polymers were synthesized with varying theoretical degrees of polymerization (DPs) [50 (small), 100 (medium), and 150 (large)] to evaluate potential effects of the polymer length in addition to grafting density. Experimental DP values were obtained via NMR end-group analysis (Figure S8). QA values were 61, 144, and 208 for small, medium, and large, respectively. M30 values were 81, 141, and 188 for small, medium, and large, respectively. These polymers underwent the same photochemical insertion reaction (Figure 3B) and were inserted onto the surface of the PCL nanofiber mats. The *grafting-to* polymer mats were prepared in a 5 mg/mL solution of polymer in MeOH as opposed to a 10 mg/mL solution used in the *grafting-from* experiments because polymers were insoluble at that concentration.

The mats were once again characterized using WCA and XPS (Figures S9 and S10). All QA and M30 mats showed the same 0° contact angle as the *grafting-from* mats; however, it was observed that complete wetting was noticeably slower than it was for the *grafting-from*-derived mats. XPS confirmed the functionalization of all mats, although intensities were much lower than the *grafting-from* mats, too low on most to gather meaningful quantitative data. This lower intensity further

https://doi.org/10.1021/acsapm.1c01264
ACS Appl. Polym. Mater. 2022, 4, 260−269

confirms the lower efficiency of *grafting-to* versus *grafting-from* chemistries.

3.4. Antibacterial Activity. Antibacterial activity of the functionalized nanofiber mats was first studied by investigating the growth of bacterial cultures that were incubated with free polymers in solution to determine efficacy (Figures S11). QA slows bacterial growth against *E. coli* at concentrations of 0.1 mg/mL and *MRSA* at concentrations of 0.5 mg/mL. M30 showed a decrease in bacterial growth against *E. coli* at concentrations of 1 mg/mL and *MRSA* at concentrations of 1 mg/mL. Solution experiments indicated that both polymers displayed antibacterial activity, with QA providing significantly enhanced efficacy against both Gram-positive and Gram-negative bacteria.

Following solution confirmation of antimicrobial activity, mats were evaluated for antibacterial activity. Mats were suspended in liquid cultures of *E. coli* and *MRSA* and were incubated for 24 h; OD measurements were taken at 600 nm (OD_{600}) at time points of 1, 3, 6, 12, and 24 h. Throughout the 24 h time course, both *E. coli* (Figure 5A) and *MRSA* (Figure 5B) showed no increase in OD with *grafting-from* antibacterial mats, indicating that these mats successfully inhibited 100% of bacterial growth. Mats incubated with *E. coli* showed a significant difference between the antibacterial (QA and M30) mats as opposed to control mats (nonfunctionalized and PEGMEA-functionalized mats), which experienced a significant amount of bacterial growth.

Mats incubated with *MRSA* showed less of a distinction between control and antibacterial mats. This is not surprising because the solution-based polymers were less potent antibacterial agents. As such, we used higher quantities of mats to elicit sufficient antibacterial activity (two 11 mm in diameter mats for *MRSA* versus one-half of a mat for *E. coli*). Using more materials created an increase in bacterial fouling of the mats; therefore, as the technology develops, it may be warranted to include antifouling monomers in our coating as well. It is important to note that the antibacterial mats are more effective than using a common antibiotic with MRSA, indicating that these materials may overcome antibacterial resistance.

The *grafting-to*-prepared mats exhibited a modest degree of inhibition of *E. coli* growth but were significantly less efficacious than the SI-ATRP-prepared mats (Figure 5C–F). The *grafting-to* PCL mats displayed an interesting phenomenon when incubated with *MRSA*, demonstrating less bacterial growth than the antibacterial mats. The PCL control mats fouled bacteria significantly more than the antibacterial mats, where the antibacterial mats seem to act in an antifouling manner. This is further amplified by the lower activity of the materials against *MRSA*, whereby two full mats were used in *MRSA* incubations as opposed to one-half of a mat for *E. coli*.

To confirm the lack of bacterial growth was due to the mats being bactericidal and not just bacteriostatic, live/dead assays were performed on *grafting-from* mats to determine whether the antibacterial fibers were cytotoxic. Only the *grafting-from* mats were chosen because of their superior antibacterial efficacy. DMAO is a green, fluorescent nucleic acid dye used to stain both live and dead bacteria, EthD-III is a red fluorescent nucleic acid dye that selectively stains dead bacteria. All control mats showed a roughly equivalent ratio of living to dead bacteria. Unmodified PCL mats showed that 58.7% of *E. coli* survived (Figure 6A), while 50.4% of *MRSA* survived (Figure 6B). Comparatively, 60.0% of *E. coli* survived when incubated with the PEGMEA-functionalized mats (Figure 6C), while 66.9% of *MRSA* survived (Figure 6D). Antibacterial nanofibers (QA and M30) showed 100% cytotoxicity after 24 h incubation with both *E. coli* and *MRSA* bacteria (Figure 6E–H).

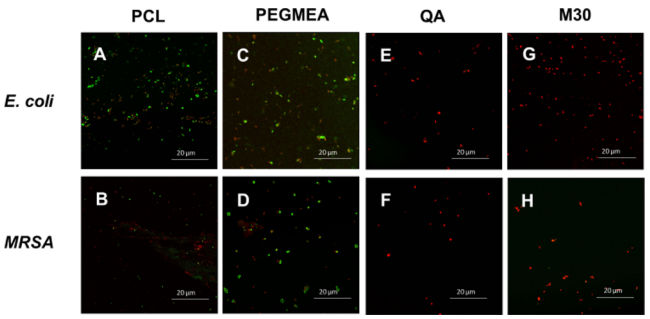

Figure 6. Antibacterial *grafting-from* fiber testing with *E. coli* (A,C,E,G) and MRSA (B,D,F,H) with live (green) and dead (red) stains after 24 h of bacterial incubation. Imaged with confocal microscopy. (A,B) PCL, (C,D) PEGMEA, (E,F) QA, (G,H) M30.

3.5. Biocompatibility. To assess the biocompatibility of antibacterial mats, NIH3T3 fibroblasts were grown for 24 and 48 h, followed by the collection of the supernatant for an LDH assay. The data are represented relative to the positive control (cell cultures with Triton X-100 in PBS) Cytotoxicity tests show no significant differences among the LDH release of cells cultured on antimicrobial versus control mats (Figure 7A). This confirms that the PCL-based substrates fabricated by extrusion were not cytotoxic to mammalian cells regardless of chemical modifications.

3.6. Profibrotic Response and Cellular Proliferation. Studies have shown that TGF-β1 released by fibroblasts contributes to various cellular processes including differentiation, proliferation, migration, and extracellular matrix remodeling. In particular, TGF-β1 influences the activation of fibroblasts into myofibroblasts, a cell phenotype with increased contractility and higher synthetic and secretory capabilities (e.g., collagens Type I, III, IV, and V, fibronectins, proteoglycans, and elastins). These responses are actively involved in tissue repair after injury.[53] Therefore, the secretion of TGF-β1 levels by fibroblasts in the supernatant was assessed together with the proliferation of cells on functionalized and nonfunctionalized mats after 24 and 48 h of cultivation (Figure S12). IFN-γ was used as a positive control because of its involvement in the upregulation of TGF-β in dermal and corneal fibroblasts.[54] As shown in Figure 7B, no statistically significant difference in TGF-β1 secretion by fibroblasts cultured on functionalized and nonfunctionalized mats was observed at both time points compared to the positive control, thus confirming that all investigated samples stimulated cellular activation into myofibroblasts and their suitability as antimicrobial bandages.[55]

It is noteworthy to highlight that cells proliferated at a slower pace on nonfunctionalized mats (i.e., PCL and PEGMEA) compared to QA- and M30-grafted substrates by analyzing the number of trypsinized cells and having assessed the detachment efficacy (Figure 7C and S13). This is in accordance with measured TGF-β1 secretion because it was reported how myofibroblastic phenotype is correlated with major collagen synthesis but a reduction in cell proliferation.[56]

https://doi.org/10.1021/acsapm.1c01264
ACS Appl. Polym. Mater. 2022, 4, 260–269

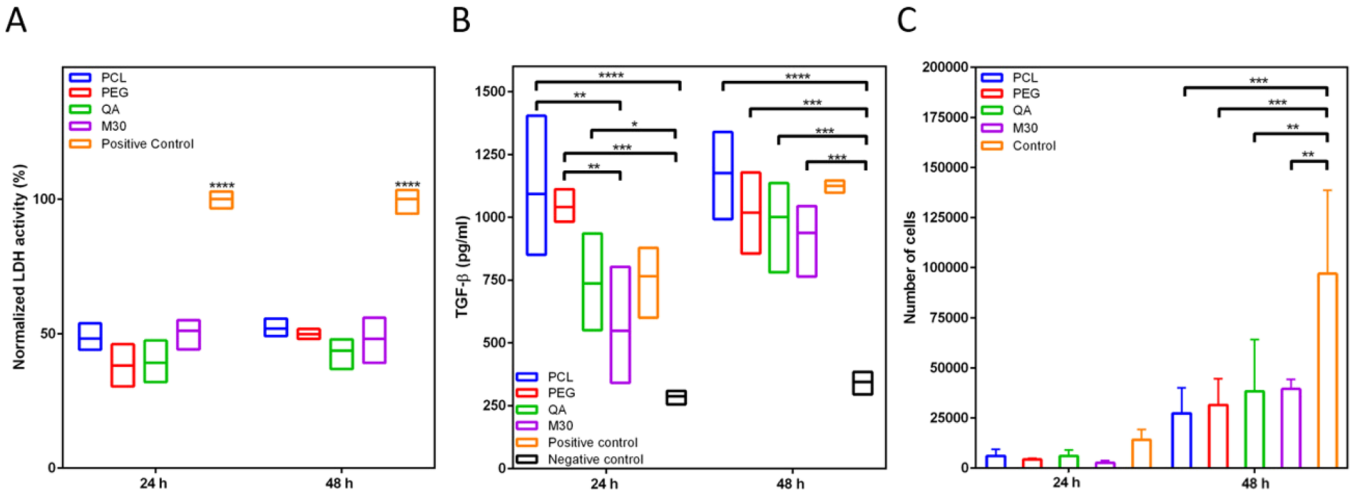

Figure 7. Biocompatibility study of antimicrobial mats (n = 3, 625 cells/mm^2). (A) Cell viability determined by LDH assay. (B) TGF-β secretion measurements. (C) Cell proliferation on mats. One-way ANOVA with Tukey's multiple test comparison was performed for assessing statistical significance,*p≤0.05, **p ≤ 0.01, ***p≤0.001 and ****p ≤ 0.0001.

4. CONCLUSIONS

This study successfully demonstrated the fabrication of antibacterial nanofiber mats from a high-throughput melt coextrusion process. Following the photochemical insertion of an ATRP initiator, *grafting-from* polymerizations were shown to be significantly more effective than their *grafting-to* counterparts at successfully killing more than 99.9% of both Gram-negative *E. coli* and Gram-positive *MRSA*. Of importance is the fact that these materials are effective against antibiotic-resistant bacteria. The mats still retained their biocompatibility and enhanced the myofibrotic response by cultured fibroblasts. This *grafting-from* method was therefore more bactericidal and less toxic than other antibacterial materials, such as biocide release or those that use a contact killing mechanism. Future work will entail creating multifunctional fiber mats including antiviral, antifungal, and blood clotting agents to create multifaceted antimicrobial materials that are low-cost, simple to manufacture, and are a competitor to traditional first aid measures.

■ ASSOCIATED CONTENT

Supporting Information

The Supporting Information is available free of charge at https://pubs.acs.org/doi/10.1021/acsapm.1c01264.

Procedures for mechanical testing; initiator and polymer synthesis; NMR of nanofibers, initiators, and polymers; SEM−EDS of PCL and initiator-functionalized PCL; TGA of PCL, QA, and M30 mats, SEM of QA and M30 mats; M_n determination of *grafting-to* polymers via NMR; water contact angles of *grafting-to* functionalized mats; XPS spectra of *grafting-to* functionalized mats; optical density measurements of bacteria with free polymers; standard curve for TGF-β1 detection; confocal laser scanning microscopy of trypsinized PCL, PEGMEA, M30, and QA mats (PDF)

■ AUTHOR INFORMATION

Corresponding Author

Jonathan K. Pokorski − *Department of NanoEngineering, University of California San Diego, Jacobs School of Engineering, La Jolla, California 92093, United States;* orcid.org/0000-0001-5869-6942; Phone: 858-246-3183; Email: jpokorski@ucsd.edu

Authors

Justin D. Hochberg − *Department of NanoEngineering, University of California San Diego, Jacobs School of Engineering, La Jolla, California 92093, United States;* orcid.org/0000-0002-9839-2836

David M. Wirth − *Department of NanoEngineering, University of California San Diego, Jacobs School of Engineering, La Jolla, California 92093, United States;* orcid.org/0000-0003-0383-7626

Giovanni Spiaggia − *Adolphe Merkle Institute, University of Fribourg, 1700 Fribourg, Switzerland;* orcid.org/0000-0001-5668-7217

Pooja Shah − *Department of NanoEngineering, University of California San Diego, Jacobs School of Engineering, La Jolla, California 92093, United States*

Barbara Rothen-Rutishauser − *Adolphe Merkle Institute, University of Fribourg, 1700 Fribourg, Switzerland;* orcid.org/0000-0002-7805-9366

Alke Petri-Fink − *Adolphe Merkle Institute, University of Fribourg, 1700 Fribourg, Switzerland;* orcid.org/0000-0003-3952-7849

Complete contact information is available at: https://pubs.acs.org/10.1021/acsapm.1c01264

Notes

The authors declare no competing financial interest.

■ ACKNOWLEDGMENTS

J.K.P., J.D.H., and D.M.W. acknowledge NSF Partnerships for International Research and Education (PIRE) for financial support (OISE 1844463). The Zhang Group and Steinmetz Group are acknowledged for supplying bacterial stocks, the S. Chen Group is acknowledged for allowing access to the uniaxial testing apparatus. The Baer Group (Cong Zhang and Xiting Wang) is acknowledged for assisting with and providing access to melt coextrusion equipment. The Maia Group (Dana Klein) is acknowledged for assisting with and providing access to a twin-screw extruder. The authors acknowledge the use of facilities and instrumentation supported by NSF through the

UC San Diego Materials Research Science and Engineering Center (UCSD MRSEC) (Ricardo De-Luna), grant # DMR-2011924." The UCSD Microscopy Core (NS04701) is acknowledged for providing access to confocal microscopes. G. S., A. P.-F., B. R.-R. gratefully acknowledge financial support from the Swiss National Science Foundation (SNSF) through the Partnerships for International Research and Education (PIRE) program under grant number IZPIP0_177995, and the Adolphe Merkle Foundation.

REFERENCES

(1) Valente, T. A. M.; Silva, D. M.; Gomes, P. S.; Fernandes, M. H.; Santos, J. D.; Sencadas, V. Effect of Sterilization Methods on Electrospun Poly(Lactic Acid) (PLA) Fiber Alignment for Biomedical Applications. *ACS Appl. Mater. Interfaces* **2016**, *8*, 3241−3249.
(2) Diao, H. J.; Wang, K.; Long, H. Y.; Wang, M.; Chew, S. Y. Highly Fluorescent and Photostable Polymeric Nanofibers as Scaffolds for Cell Interfacing and Long-Term Tracking. *Adv. Healthcare Mater.* **2016**, *5*, 529−533.
(3) Nagiah, N.; Johnson, R.; Anderson, R.; Elliott, W.; Tan, W. Highly Compliant Vascular Grafts with Gelatin-Sheathed Coaxially Structured Nanofibers. *Langmuir* **2015**, *31*, 12993−13002.
(4) Jordan, A. M.; Viswanath, V.; Kim, S.-E.; Pokorski, J. K.; Korley, L. T. J. Processing and Surface Modification of Polymer Nanofibers for Biological Scaffolds: A Review. *J. Mater. Chem. B* **2016**, *4*, 5958−5974.
(5) Smith Callahan, L. A.; Xie, S.; Barker, I. A.; Zheng, J.; Reneker, D. H.; Dove, A. P.; Becker, M. L. Directed Differentiation and Neurite Extension of Mouse Embryonic Stem Cell on Aligned Poly(Lactide) Nanofibers Functionalized with YIGSR Peptide. *Biomaterials* **2013**, *34*, 9089−9095.
(6) Chen, F.; Hochleitner, G.; Woodfield, T.; Groll, J.; Dalton, P. D.; Amsden, B. G. Additive Manufacturing of a Photo-Cross-Linkable Polymer via Direct Melt Electrospinning Writing for Producing High Strength Structures. *Biomacromolecules* **2016**, *17*, 208−214.
(7) Zuo, F.; Tan, D. H.; Wang, Z.; Jeung, S.; Macosko, C. W.; Bates, F. S. Nanofibers from Melt Blown Fiber-in-Fiber Polymer Blends. *ACS Macro Lett.* **2013**, *2*, 301−305.
(8) Badrossamay, M. R.; McIlwee, H. A.; Goss, J. A.; Parker, K. K. Nanofiber Assembly by Rotary Jet-Spinning. *Nano Lett.* **2010**, *10*, 2257−2261.
(9) Badrossamay, M. R.; Balachandran, K.; Capulli, A. K.; Golecki, H. M.; Agarwal, A.; Goss, J. A.; Kim, H.; Shin, K.; Parker, K. K. Engineering Hybrid Polymer-Protein Super-Aligned Nanofibers via Rotary Jet Spinning. *Biomaterials* **2014**, *35*, 3188−3197.
(10) Wang, J.; Langhe, D.; Ponting, M.; Wnek, G. E.; Korley, L. T. J.; Baer, E. Manufacturing of Polymer Continuous Nanofibers Using a Novel Co-Extrusion and Multiplication Technique. *Polymer* **2014**, *55*, 673−685.
(11) Wang, N.; Burugapalli, K.; Song, W.; Halls, J.; Moussy, F.; Zheng, Y.; Ma, Y.; Wu, Z.; Li, K. Tailored Fibro-Porous Structure of Electrospun Polyurethane Membranes, Their Size-Dependent Properties and Trans-Membrane Glucose Diffusion. *J. Membr. Sci.* **2013**, *427*, 207−217.
(12) Camerlo, A.; Bühlmann-Popa, A.-M.; Vebert-Nardin, C.; Rossi, R. M.; Fortunato, G. Environmentally Controlled Emulsion Electrospinning for the Encapsulation of Temperature-Sensitive Compounds. *J. Mater. Sci.* **2014**, *49*, 8154−8162.
(13) Esmaeilzadeh, I.; Mottaghitalab, V.; Tousifar, B.; Afzali, A.; Lamani, M. A Feasibility Study on Semi Industrial Nozzleless Electrospinning of Cellulose Nanofiber. *Int. J. Ind. Chem.* **2015**, *6*, 193−211.
(14) Kim, S.-E.; Jordan, A. M.; Korley, L. T. J.; Pokorski, J. K. Drawing in Poly (ε-Caprolactone) Fibers: Tuning Mechanics, Fiber Dimensions and Surface-Modification Density. *J. Mater. Chem. B* **2017**, *5*, 4499−4506.
(15) Kim, S.-E.; Wang, J.; Jordan, A. M.; Korley, L. T. J.; Baer, E.; Pokorski, J. K. Surface Modification of Melt Extruded Poly(ε-Caprolactone) Nanofibers: Toward a New Scalable Biomaterial Scaffold. *ACS Macro Lett.* **2014**, *3*, 585−589.
(16) Kim, S.-E.; Zhang, C.; Advincula, A. A.; Baer, E.; Pokorski, J. K. Protein and Bacterial Antifouling Behavior of Melt-Coextruded Nanofiber Mats. *ACS Appl. Mater. Interfaces* **2016**, *8*, 8928−8938.
(17) Kim, S.-E.; Harker, E. C.; De Leon, A. C.; Advincula, R. C.; Pokorski, J. K. Coextruded, Aligned, and Gradient-Modified Poly(ε-Caprolactone) Fibers as Platforms for Neural Growth. *Biomacromolecules* **2015**, *16*, 860−867.
(18) Cortizo, M. S.; Molinuevo, M. S.; Cortizo, A. M. Biocompatibility and Biodegradation of Polyester and Polyfumarate Based-Scaffolds for Bone Tissue Engineering. *J. Tissue Eng. Regen. Med.* **2008**, *2*, 33−42.
(19) Mei, N.; Chen, G.; Zhou, P.; Chen, X.; Shao, Z.-Z.; Pan, L.-F.; Wu, C.-G. Biocompatibility of Poly(ε-Caprolactone) Scaffold Modified by Chitosan—The Fibroblasts Proliferation in Vitro. *J. Biomater. Appl.* **2005**, *19*, 323−339.
(20) Park, H.-S.; Gong, M.-S.; Knowles, J. C. Synthesis and Biocompatibility Properties of Polyester Containing Various Diacid Based on Isosorbide. *J. Biomater. Appl.* **2012**, *27*, 99−109.
(21) Nair, L. S.; Laurencin, C. T. Biodegradable Polymers as Biomaterials. *Prog. Polym. Sci.* **2007**, *32*, 762−798.
(22) Gunatillake, P.; Mayadunne, R.; Adhikari, R. Recent Developments in Biodegradable Synthetic Polymers. In *Biotechnology Annual Review*; Elsevier, 2006; Vol. *12*, pp. 301−347.
(23) Centers for Disease Control and Prevention (U.S.). *Antibiotic Resistance Threats in the United States, 2019*; Centers for Disease Control and Prevention (U.S.), 2019.
(24) Vinh, D. C.; Embil, J. M. Rapidly Progressive Soft Tissue Infections. *Lancet Infect. Dis.* **2005**, *5*, 501−513.
(25) DiNubile, M. J. Complicated Infections of Skin and Skin Structures: When the Infection Is More than Skin Deep. *J. Antimicrob. Chemother.* **2004**, *53*, ii37−ii50.
(26) Sukumaran, V.; Senanayake, S. Bacterial Skin and Soft Tissue Infections. *Aust. Prescr.* **2016**, *39*, 159−163.
(27) Kurtz, I.; Schiffman, J. Current and Emerging Approaches to Engineer Antibacterial and Antifouling Electrospun Nanofibers. *Materials* **2018**, *11*, 1059.
(28) Kayaci, F.; Umu, O. C. O.; Tekinay, T.; Uyar, T. Antibacterial Electrospun Poly(Lactic Acid) (PLA) Nanofibrous Webs Incorporating Triclosan/Cyclodextrin Inclusion Complexes. *J. Agric. Food Chem.* **2013**, *61*, 3901−3908.
(29) Rieger, K. A.; Schiffman, J. D. Electrospinning an Essential Oil: Cinnamaldehyde Enhances the Antimicrobial Efficacy of Chitosan/Poly(Ethylene Oxide) Nanofibers. *Carbohydr. Polym.* **2014**, *113*, 561−568.
(30) Ignatova, M.; Manolova, N.; Markova, N.; Rashkov, I. Electrospun Non-Woven Nanofibrous Hybrid Mats Based on Chitosan and PLA for Wound-Dressing Applications. *Macromol. Biosci.* **2009**, *9*, 102−111.
(31) Nguyen, T.-H.; Kim, Y.-H.; Song, H.-Y.; Lee, B.-T. Nano Ag Loaded PVA Nano-Fibrous Mats for Skin Applications. *J. Biomed. Mater. Res., Part B* **2011**, *96B*, 225−233.
(32) Schiffman, J. D.; Wang, Y.; Giannelis, E. P.; Elimelech, M. Biocidal Activity of Plasma Modified Electrospun Polysulfone Mats Functionalized with Polyethyleneimine-Capped Silver Nanoparticles. *Langmuir* **2011**, *27*, 13159−13164.
(33) Rieger, K. A.; Cho, H. J.; Yeung, H. F.; Fan, W.; Schiffman, J. D. Antimicrobial Activity of Silver Ions Released from Zeolites Immobilized on Cellulose Nanofiber Mats. *ACS Appl. Mater. Interfaces* **2016**, *8*, 3032−3040.
(34) Lin, N.; Berton, P.; Moraes, C.; Rogers, R. D.; Tufenkji, N. Nanodarts, Nanoblades, and Nanospikes: Mechano-Bactericidal Nanostructures and Where to Find Them. *Adv. Colloid Interface Sci.* **2018**, *252*, 55−68.
(35) Schiffman, J. D.; Elimelech, M. Antibacterial Activity of Electrospun Polymer Mats with Incorporated Narrow Diameter Single-Walled Carbon Nanotubes. *ACS Appl. Mater. Interfaces* **2011**, *3*, 462−468.

(36) Zasloff, M. Antimicrobial Peptides of Multicellular Organisms. *Nature* **2002**, *415*, 389−395.
(37) Yeaman, M. R.; Yount, N. Y. Mechanisms of Antimicrobial Peptide Action and Resistance. *Pharmacol. Rev.* **2003**, *55*, 27−55.
(38) Brogden, K. A. Antimicrobial Peptides: Pore Formers or Metabolic Inhibitors in Bacteria? *Nat. Rev. Microbiol.* **2005**, *3*, 238−250.
(39) Paslay, L. C.; Abel, B. A.; Brown, T. D.; Koul, V.; Choudhary, V.; McCormick, C. L.; Morgan, S. E. Antimicrobial Poly(Methacrylamide) Derivatives Prepared via Aqueous RAFT Polymerization Exhibit Biocidal Efficiency Dependent upon Cation Structure. *Biomacromolecules* **2012**, *13*, 2472−2482.
(40) Teuber, M.; Bader, J. Action of Polymyxin B on Bacterial Membranes: Morphological Changes in the Cytoplasm and in the Outer Membrane of Salmonella Typhimurium and *Escherichia coli* B. *Arch. Microbiol.* **1976**, *109*, 8.
(41) Parandhaman, T.; Choudhary, P.; Ramalingam, B.; Schmidt, M.; Janardhanam, S.; Das, S. K. Antibacterial and Antibiofouling Activities of Antimicrobial Peptide-Functionalized Graphene−Silver Nanocomposites for the Inhibition and Disruption of *Staphylococcus Aureus* Biofilms. *ACS Biomater. Sci. Eng.* **2021**, 1c01253.
(42) Wuersching, S. N.; Huth, K. C.; Hickel, R.; Kollmuss, M. Inhibitory Effect of LL-37 and Human Lactoferricin on Growth and Biofilm Formation of Anaerobes Associated with Oral Diseases. *Anaerobe* **2021**, *67*, 102301.
(43) Kumar, A.; Boyer, C.; Nebhani, L.; Wong, E. H. H. Highly Bactericidal Macroporous Antimicrobial Polymeric Gel for Point-of-Use Water Disinfection. *Sci. Rep.* **2018**, *8*, 7965.
(44) Zuo, H.; Wu, D.; Fu, R. Synthesis of Antibacterial Polymers from 2-Dimethylamino Ethyl Methacrylate Quaternized by Dimethyl Sulfate. *Polym. J.* **2010**, *42*, 766−771.
(45) Cuthbert, T. J.; Hisey, B.; Harrison, T. D.; Trant, J. F.; Gillies, E. R.; Ragogna, P. J. Surprising Antibacterial Activity and Selectivity of Hydrophilic Polyphosphoniums Featuring Sugar and Hydroxy Substituents. *Angew. Chem., Int. Ed.* **2018**, *57*, 12707−12710.
(46) Judzewitsch, P. R.; Corrigan, N.; Trujillo, F.; Xu, J.; Moad, G.; Hawker, C. J.; Wong, E. H. H.; Boyer, C. High-Throughput Process for the Discovery of Antimicrobial Polymers and Their Upscaled Production via Flow Polymerization. *Macromolecules* **2020**, *53*, 631−639.
(47) Sato, T.; Dunderdale, G. J.; Hozumi, A. Simple and Scalable Protocol for Producing Hydrophobic Polymer Brushes Beyond Wafer-Scale Dimensions toward Real-Life Applications. *ACS Appl. Polym. Mater.* **2021**, *3*, 1395−1405.
(48) Ziemann, E.; Coves, T.; Levin, O.; Bernstein, R. Zwitterion Polymer Brushes on Porous Membranes: Characterization, Tribology, Performance, and the Effect of Electrolyte Anions. *ACS Appl. Polym. Mater.* **2020**, *2*, 4613−4625.
(49) Rubio, N.; Au, H.; Leese, H. S.; Hu, S.; Clancy, A. J.; Shaffer, M. S. P. Grafting from versus Grafting to Approaches for the Functionalization of Graphene Nanoplatelets with Poly(Methyl Methacrylate). *Macromolecules* **2017**, *50*, 7070−7079.
(50) Jordan, A. M.; Korley, L. T. J. Toward a Tunable Fibrous Scaffold: Structural Development during Uniaxial Drawing of Coextruded Poly(ε-Caprolactone) Fibers. *Macromolecules* **2015**, *48*, 2614−2627.
(51) Kósa, C.; Sedlačík, M.; Fiedlerová, A.; Chmela, Š.; Borská, K.; Mosnáček, J. Photochemically Cross-Linked Poly(ε-Caprolactone) with Accelerated Hydrolytic Degradation. *Eur. Polym. J.* **2015**, *68*, 601−608.
(52) Liu, P.; Su, Z. Surface-Initiated Atom Transfer Radical Polymerization (SI-ATRP) of Styrene from Chitosan Particles. *Mater. Lett.* **2006**, *60*, 1137−1139.
(53) Negmadjanov, U.; Godic, Z.; Rizvi, F.; Emelyanova, L.; Ross, G.; Richards, J.; Holmuhamedov, E. L.; Jahangir, A. TGF-B1-Mediated Differentiation of Fibroblasts Is Associated with Increased Mitochondrial Content and Cellular Respiration. *PLoS One* **2015**, *10*, No. e0123046.
(54) Sung, J. Y.; Yoon, K.; Ye, S.-K.; Goh, S.-H.; Park, S.-Y.; Kim, J. H.; Kang, H. G.; Kim, Y.-N.; Park, B.-K. Upregulation of Transforming Growth Factor-Beta Type I Receptor by Interferon Consensus Sequence-Binding Protein in Osteosarcoma Cells. *Biochim. Biophys. Acta, Mol. Cell Res.* **2019**, *1866*, 761−772.
(55) Gilbert, R.; Vickaryous, M.; Viloria-Petit, A. Signalling by Transforming Growth Factor Beta Isoforms in Wound Healing and Tissue Regeneration. *J. Dev. Biol.* **2016**, *4*, 21.
(56) Grotendorst, G. R.; Rahmanie, H.; Duncan, M. R. Combinatorial Signaling Pathways Determine Fibroblast Proliferation and Myofibroblast Differentiation. *FASEB J.* **2004**, *18*, 469−479.

https://doi.org/10.1021/acsapm.1c01264
ACS Appl. Polym. Mater. 2022, 4, 260−269